Paper-ID: VGI_197208

On Model Formation With Remote Sensing Imagery

Franz Leberl [1]

[1] *Internat. Instit. f. Aerial Survey and Earth Sciences (ITC), Enschede (the Netherlands)*

Österreichische Zeitschrift für Vermessungswesen **60** (2), S. 43–61

1972

BibTEX:

```
@ARTICLE{Leberl_VGI_197208,
Title =  {On Model Formation With Remote Sensing Imagery},
Author =  {Leberl, Franz},
Journal =  {{\"O}sterreichische Zeitschrift f{\"u}r Vermessungswesen},
Pages =  {43--61},
Number =  {2},
Year =  {1972},
Volume =  {60}
}
```

Nehmen wir an, der mittlere Fehler des Winkels zwischen Sonne und einem Flugzeug wäre $\pm$ 15″ und der mittlere Fehler nach Gl. (11) abgeschätzt wäre $\pm$ 10″, dann wäre der Fehler einer Azimutmessung

$$\sqrt{15^2 + 10^2} = \pm 18''$$

Beachtet man noch, daß in jedem der drei Standpunkte die Azimutmessung erfolgt, d. h. für jede der drei Seiten zweimal die Azimute fast unabhängig voneinander bestimmt werden, so folgt der mittlere azimutale Fehler des Standpunktdreiecks mit $\pm$ 18″: $\sqrt{6} \doteq \pm$ 10″.

Abschließend vergleichen wir noch eine terrestrische Trilateration bzw. Triangulation mit dem beschriebenen Verfahren. Wir können feststellen, daß die terrestrischen Verfahren zwar höchste Genauigkeit erreichen, daß sie aber einen gewaltigen Aufwand von Zeit und Arbeit für die Erkundung, für den Signalbau, für die Durchführung der Vermessung, für die Stabilisierung und für die Luftsichtbarmachung beanspruchen. Die Trilateration in der Luft erfordert zwar einen ungewöhnlich hohen technischen Aufwand, aber in vielen Fällen wird dieser Aufwand im Vergleich zur erreichbaren Leistung nur sehr gering zu bewerten sein.

Literatur

[1] *Cesàro, E.:* Vorlesungen über natürliche Geometrie, Verlag Teubner, 1901

[2] *Duda, Th.:* Flugzeuggeräte Bd. 1, 2 VED Verlag Technik Berlin 1959

[3] *Hesse, W.:* Handbuch der Aerologie, Akademische Verlagsgesellschaft 1961

[4] *Killian, K.:* Vorschläge zur räumlichen Aerotriangulation, Ö.Z.f.V., 56. Jahrgang, Nr. 3 (1968)

[5] *Koschmieder, H.:* Dynamische Meteorologie, 3. Aufl., Akademische Verlagsgesellschaft, 1951

[6] *Linke, F.:* Meteorologisches Taschenbuch IV, Akademische Verlagsgesellschaft, 1943.

[7] *Mühlig, F.:* Astronomisch-geodätische Ortsbestimmung, Verlag Herbert Wichmann, 1960.

[8] *Müller, G.* u. *Reinhardt, M.:* Zur Bestimmung atmosphärischer Parameter bei Flugzeugmessungen, Z. Flugwissenschaft 14 (1966), Heft 2.

[9] *Philipps, H.:* Gradientwind-Nomogramm, Z. f. Meteorologie, 1, 1947.

[10] *Raethjen, P.:* Physik der Atmosphäre, 1. u. 2. Bd., Verlag Teubner, 1942.

[11] *Scherhag, R.:* Wetteranalyse und Wetterprognose, Verlag Springer, 1948.

On Model Formation With Remote Sensing Imagery

By *F. Leberl*, Enschede (The Netherlands)

1. *Introduction*

The imaging remote sensing systems on which the photogrammetric interest is presently focussed, are enumerated in table 1. Not considering the conventional frame camera, the number of contributions in the open literature to the problem of deriving object-space coordinates from remote sensing imagery is rather small.

However, for a number of systems of table 1, model formation with remote sensing imagery has been discussed. An excellent review of the state of the art was

given by Konecny in [5]. As concerns panoramic and continuous strip photography, a basis was established by Case [1]. Derenyi's study [2], which concerns the relative orientation of continuous strip photography, can be generalized to imagery obtained from the recti-linearly scanning optical-mechanical sensor, as it is presently applied for Multispectral Sensing (MSS) and Infrared Linescanning (IRLS). With regard to imagery from the Plan Position Indicator (PPI), reference has to be made to the book of D. Levine on radargrammetry [8], in which the concept of a PPI-stereoplotter is described.

Model formation with Side-Looking Airborne Radar (SLAR) imagery has been tried by Laprade, using the visually perceived parallax in a analogue manner [7], [8]. Based on this, Goodyear developped an automatic analogue stereoplotter [12], [15]. Recently it has been reported, that also the AS-11A Analytical Plotter could be successfully applied to the mapping from overlapping SLAR-imagery (Norvelle [13]). A numerical investigation on the propagation of error of the measured slant range into the model coordinates was performed by Rosenfield in [14]. The concept

I	Conventional Frame Camera
II	Panoramic Camera 1. Scanning in a plane perpendicular to the flight direction (vertical mode, rectilinear scan) 2. Scanning in a plane forming an angle $\varphi_0 \neq 90^0$ with the flight direction (oblique mode)
III	Continuous Strip Photography 1. Imaging in a plane perpendicular to flight direction (vertical mode) 2. Imaging in a plane forming an angle $\varphi_0 \neq 90^0$ with the flight direction (oblique mode)
IV	Optical-Mechanical Scanning 1. In a plane perpendicular to flight direction (vertical mode) 2. In a plane not perpendicular to flight direction (oblique mode, rectilinear scan) 3. In a cone with flight direction as axis (oblique mode, hyperbolic scan) 4. In a cone with vertical axis (circular scanning)
V	Echotime Measurement with Plan Position Indicator
VI	Side-Looking Echotime Measurement 1. In a plane perpendicular to flight direction 2. In a plane not perpendicular to flight direction (oblique mode, rectilinear scan) 3. In a cone with flight direction as axis (oblique mode, hyperbolic scan)

Table 1: Imaging remote sensing systems of prime photogrammetric interest

of combining simultaneous SLAR- and IRLS-imagery for model-formation has been published by Moore [10].

Except for Rosenfield's paper [14], no contribution is known to the author regarding the effect of an erroneous set of imaging parameters and of flight configurations onto the accuracy of model coordinates. In this paper, therefore, we will deal to a limited extent with the cofactors of model coordinates as derived from overlapping remote sensing imagery.

But first, the projection equations for the systems of table 1 are given in the following. After this, various flight configurations to obtain overlapping imagery and problems with the acquisition of imaging parameters are briefly discussed. Finally, the description and discussion of the results of a numerical investigation of the error propagation into the projection equations serves to evaluate qualitatively and quantitatively a number of various flight configurations proposed.

2. *Projection equation for remote-sensing-imagery*

It is possible to give a general projection equation for remote-sensing imagery, and to specialize this equation for the various cases of table 1 such as to get the formulae as given in [5].

The general projection equation is

$$\mathbf{X}_p = \mathbf{X}_0 + \mathbf{C}(\mathbf{B}.\mathbf{A}.\mathbf{u} + \Delta\overline{\mathbf{X}}) \qquad \ldots (1\,a)$$

or explicitely:

$$\begin{bmatrix} X \\ Y \\ Z \end{bmatrix}_p = \begin{bmatrix} X \\ Y \\ Z \end{bmatrix}_0 + \mathbf{C}\left\{\mathbf{B}.\,\mathbf{A}.\begin{bmatrix} u \\ v \\ w \end{bmatrix} + \begin{bmatrix} \Delta\overline{X} \\ \Delta\overline{Y} \\ \Delta\overline{Z} \end{bmatrix}\right\} \qquad \ldots (1\,b)$$

In this equation the vector $\mathbf{X}_p$ defines the model point and $\mathbf{X}_0$ the origin of the coordinate-system of the sensor platform, i. e. of the aircraft, satellite or ship, with respect to a cartesian terrain or model system. $\mathbf{u}$ is the vector of the modelpoint in the sensor's coordinate system, and $\Delta\overline{\mathbf{X}}$ the vector between the origin of the platform and the sensor systems, but in the platform-system (see figure 1).

$\mathbf{A}$ is the orthogonal matrix, which rotates the sensor system into the one of the sensor's mounting. $\mathbf{B}$ rotates the mounting system into the platform-system, and $\mathbf{C}$ is the exterior orientation of the platform (in particular the aircraft) in the model coordinate system.

In table 2 the specialisations of the general projection equation for the various imaging systems are summarized. In this, λ represents a scale factor, $\mathbf{E}$ the unit matrix, x, y the image coordinates, c the camera principal distance, Φ_0 the "squint", i. e. the complement to 90^0 of half the vertex angle of the cone, in which scanning is done. s is the slant range and also the length of the vector $\mathbf{u}$. $\overline{\Omega}$ is the depression angle as measured from the uv-plane to the "line of sight" between the sensor and the object. $\overline{\Omega}^*$ is the depression angle formed between the projection of the line of sight into the vw-plane and the v-coordinate axis.

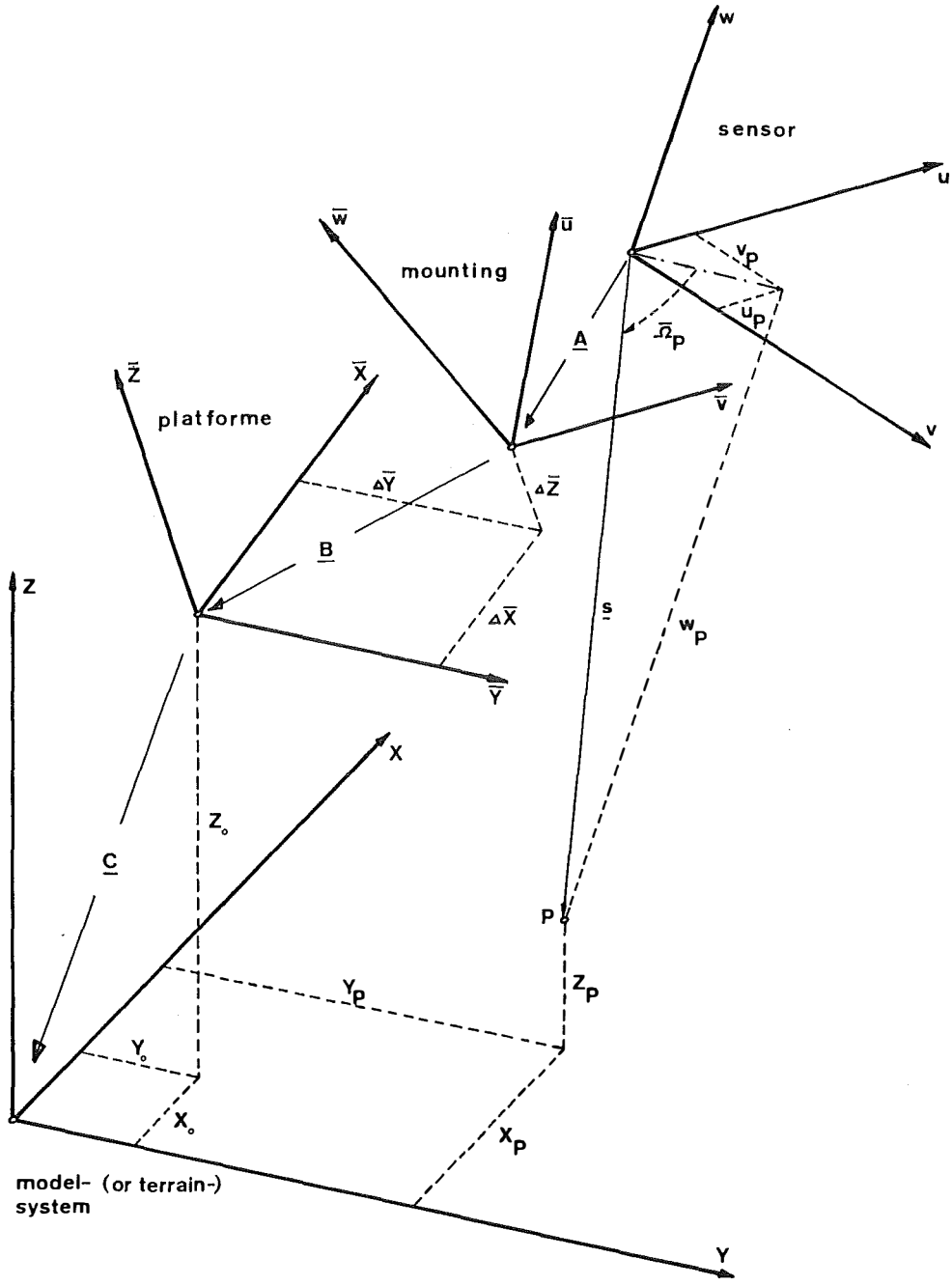

Figure 1: Coordinate systems used in equation (1)

Whereas the matrix **C** has the conventional appearance and represents the photogrammetric rotations φ, ω, $\varkappa$, one has to write for **B**:

$$\mathbf{B} = \begin{bmatrix} \cos\varphi_0 & 0 & -\sin\varphi_0 \\ 0 & 1 & 0 \\ \sin\varphi_0 & 0 & \cos\varphi_0 \end{bmatrix}$$

So **B** allows for "stereosystems" with an angle of convergence of $2 \cdot \varphi_0$.

I	$\mathbf{u} = \lambda\,(x, y, -c)^T$	$\mathbf{A} = \mathbf{E}$
II	$\mathbf{u} = \lambda\,(x, +c.\cos\overline{\Omega}^*, -c.\sin\overline{\Omega}^*)^T$	$\Omega^* = \overline{90}^\circ - y/c$
1.	$\mathbf{A} = \mathbf{B} = \mathbf{E}$	$\mathbf{E}$ = identity or unit
2.	$\mathbf{A} = \mathbf{E}$; $\mathbf{B} \neq \mathbf{E}$	matrix
III	$\mathbf{u} = (o, y, -c)^T.\lambda$	
1.	$\mathbf{A} = \mathbf{B} = \mathbf{E}$	
2.	$\mathbf{A} = \mathbf{E}$ $\mathbf{B} \neq \mathbf{E}$	
IV	$\mathbf{u} = \lambda\,(\sin\Phi_0, \cos\Phi_0.\cos\overline{\Omega}^*, \cos\Phi_0.\sin\overline{\Omega}^*)^T.c$	$\mathbf{A} = \mathbf{E}$ $\Omega^* = \overline{90}^\circ - y/c$
1.	$\Phi_0 = o$ $\mathbf{B} = \mathbf{E}$	
2.	$\Phi_0 = o$ $\mathbf{B} \neq \mathbf{E}$	
3.	$\Phi_0 \neq o$ $\mathbf{B} = \mathbf{E}$	
4.	$\Phi_0 \neq o$ $\mathbf{B} \neq \mathbf{E}$ (corresponds to $\varphi_0 = -\pi/2$)	
V	$\mathbf{u} = s.\,(\cos\alpha.\cos\overline{\Omega},\ \sin\alpha.\cos\overline{\Omega},\ \sin\overline{\Omega})^T$	$\mathbf{A} = \mathbf{E}$
VI	$\mathbf{u} = s.\,(\sin\Phi_0,\ (\cos^2\overline{\Omega} - \sin^2\Phi_0)^{1/2},\ \sin\overline{\Omega})^T$	$\mathbf{A} \neq \mathbf{E}$
1.	$\Phi_0 = o$ $\mathbf{B} = \mathbf{E}$	
2.	$\Phi_0 = o$ $\mathbf{B} \neq \mathbf{E}$	
3.	$\Phi_0 \neq o$ (formulation of Hockeborn [4])	

Table 2: Special cases as derived from general projection equation (1) for the sensing systems given in table 1

For system IV/4 in table 1, i. e. the circular scanning,

$$\mathbf{B} = \begin{bmatrix} 0 & 0 & 1 \\ 0 & 1 & 0 \\ -1 & 0 & 0 \end{bmatrix}$$

For the side-looking echotime measurement (case VI), thus for SLAR (or SONAR), it can be shown, that for $\Delta\overline{\mathbf{X}} = (0, 0, 0)$:

$$u^2 + v^2 + w^2 = s^2 = (X_p - X_0)^2 + (Y_p - Y_0)^2 + (Z_p - Z_0)^2 \qquad \ldots \text{ (2a)}$$

and

$$\tan \Phi_0 = \frac{d_{11}.(X_p - X_0) + d_{12}.(Y_p - Y_0) + d_{13}.(Z_p - Z_0)}{\left(\sum_{i=2}^{3} [d_{i,1}.(X_p - X_0) + d_{i,2}.(Y_p - Y_0) + d_{i,3}.(Z_p - Z_0)]^2 \right)^{1/2}} \quad \ldots \text{(2b)}$$

with

$$\mathbf{D} = \mathbf{A}^T.\mathbf{B}^T.\mathbf{C}^T$$

This is the formulation as used in e. g. [14].

3. *Model formation*

In the projection equation (1), two groups of parameters occur: one can be measured before the flight (pre-flight calibration), and the second depends on the exterior orientation of the sensor and location of the object point. In another way the parameters of equation (1) are for each sensor to be classified as given (observed) or as to be derived from the imagery.

There is a main difference between the direction-measuring and the echotime-measuring systems. This is because there is in the first group of systems (I—IV) an unknown scale factor λ, and in the second group (V—VI) the unknown depression angle $\overline{\Omega}$ to be determined, in addition to the inner and exterior orientation as well as the object space — or model coordinates.

3.1 *On the determination of the elements of exterior orientation*

The question arises as to how to determine the exterior orientation, which is variable within the imagery taken by systems of type II to VI. There are the following possibilities:

relative orientation
measurement
estimation with the help of control points
assuming an ideal path and orientation of the sensor.

The photogrammetric method of relative orientation to obtain data of exterior orientation by a triangulation in space is to be applied in the first instance to overlapping images of category I and II only. In an extensive investigation on continuous strip photography, however, Derenyi concludes in [2], that a somewhat satisfactory relative orientation for the purpose of triangulation is only possible with this type of imagery if two convergent (type III/2) strip cameras are combined with one of type III/1 (see for this also Konecny [5] and Masry [9]).

The continuous strip of imagery is thereby cut in pieces along the flight line, so that the random functions of the elements of exterior orientation can be approximated within a piece by simple polynomials of first or second order. The procedure of relatively orienting on piece of imagery to the previous one produces the exterior orientation as group of joint polynomials.

Generalizing the experimental results as obtained by Derenyi for the case of strip-photography in such a way that they are also valid for other imaging systems

with comparatively severely reduced geometric resolution, one must conclude that the method of relative orientation cannot produce better but rather inferior results as compared to the direct measurement during flight. This is due to the mean square error of unit weight, σ_0, which is large in systems IV—VI as compared to strip photography.

The method of relative orientation cannot be applied to overlapping imagery taken in different flight-lines to obtain exterior orientation, because there is no possibility to perform a (numerical) "triangulation" by means of pieces of imagery, so that measurement is a good though expensive alternative.

The use of control points in a plotting procedure is better not tried for the determination of the elements of exterior orientation, since the number of unknowns is impractically large (matrix $\mathbf{C}$ and vector $\mathbf{X}_0$ in (1)). In the case that control points are given it is considered to be more practical to compute model coordinates under the assumption of an idealized exterior orientation and to improve these preliminary model coordinates with an interpolation method. In this last procedure, only three entities are interpolated, namely the errors in the three model coordinates. This seems more favourable than interpolation of the 12 elements of exterior orientation.

The unknowns of the exterior orientation could also be derived from simultaneous exposures with a frame camera, by applying aerial triangulation. This auxiliary photography would first give values for the exterior orientation at discrete points along the flight line. It could also be applied for an orientation of the continuous imagery using areas of common overlap between the frame and continuous imagery. This concept may seem contradictory, since frame photography should make continuous imagery unnecessary, at least from a photogrammetric point of view. But there is the case, as in the SLAR-Project RADAM in Brasil [11], that frame photography is taken anyway together with SLAR. Due to cloud cover, the frame photography may then just be used to improve the data of exterior orientation. Plotting, however, would have to be done from SLAR.

3.2 *Flight configurations*

The standard input for conventional photogrammetric model formation consists of overlapping photographs taken along one flight line. This is generally not possible with systems of the categories III to VI, but only in a special case of convergent sensors with $\Phi_0 \neq 0$ and/or $\mathbf{B} \neq \mathbf{E}$. Mostly, however, the imagery to be used for plotting will be produced along separate flight lines. It is therefore necessary to consider the possibilities and alternatives to obtain overlaps and to study their consequences.

Figure 2 shows the idealized sketches of a number of flight configurations allowing for producing overlapping imagery. The most interesting is variant (a), since it can (under certain restrictions, see 3.1) enable a triangulation to be carried out. With the systems III, IV and VI, which in a very short period of time only image a line of the object space, this scheme (a) is only possible with convergent sensors, thus with optical axes that are directed forward and backward. There is one exception: the side-looking echotime measurement with forward and backward directed conical

impulses does not allow the derivation of model-coordinates. This is because the imagery from each impulse defines a circle which is concentric with respect to the flight line. The two circles will by necessity be coincident (having same center and equal radii) and would define no specific points of intersection. Therefore, a "stereo-SLAR-system" with alternately emitting conical impulses in forward and backward directions does not fulfill its purpose. Only plane convergent impulses could make up a meaningful stereo-SLAR-system. (The two circles will in this case be in two inclined planes, thus intersecting in unique point(s).)

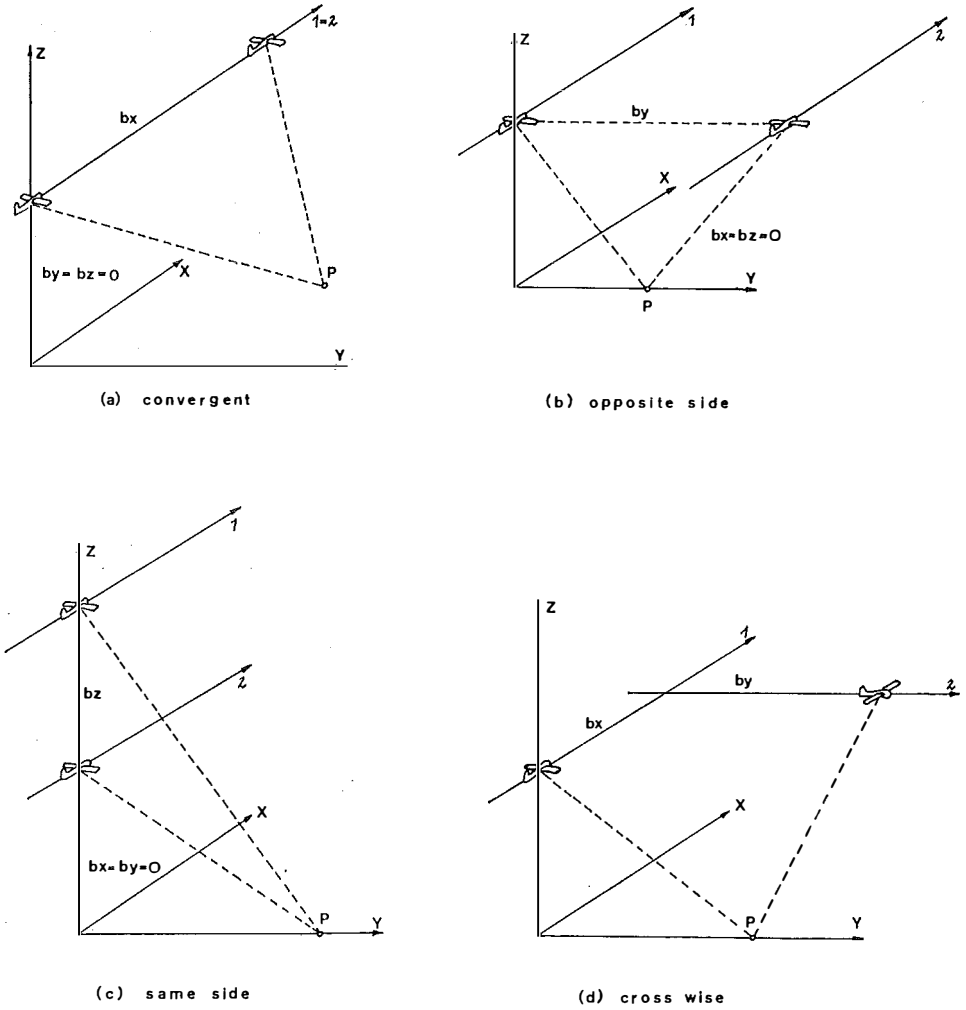

Figure 2: Idealized flight configurations to obtain overlapping imagery

With reference to optical-mechanical scanning both concepts of convergence (conical and plane) define a model point(s). The hyperbolic scan, however, produces more accurate heights, as can be found from the propagation of the mean error of measurement of image coordinates, σ_0.

Two convergent plane scans produce a height error:

$$m'_H = \frac{H.(\cos^2\varphi_0.\tan^2\Omega_B/2+1)^{1/2}.\sigma_0}{c.\sin\varphi_0} \quad H \ldots \text{flight height}$$

whereas two convergent scanning cones give:

$$m''_H = \frac{H.(\cos^2\Omega+1)^{1/2}.\sigma_0}{\sqrt{2}.\sin\Phi_0.c} \text{ (for derivation see Appendix)}$$

In other words: the hyperbolic scan (= scanning cone) allows for a better base-height ratio with increasing distance from the flight line, so that $m''_H < m'_H$ for $\Omega > 0$.

3.3 *Computation of model coordinates*

Assuming that the parameters for the inner and exterior orientation are known, then each image point P' is producing one set of three equations (type (1)) with four unknowns: X, Y, Z, λ' for direction measuring systems, and X, Y, Z, $\overline{\Omega}'$ for echotime measuring systems. If the point P is imaged another time also, then once again three equations are produced, in which only λ'' or $\overline{\Omega}''$ is added as new unknown. So the computation of modelcoordinates represents an overdetermined problem.

Formulation of the computation of the model coordinates by means of the two sets of equations of type (1) gives thus 6 equations with 5 unknowns. Elimination of the model coordinates results in the coplanarity condition:

$$\mathbf{C}'(\mathbf{B}.\mathbf{A}.\mathbf{u}' + \Delta\overline{\mathbf{X}}) - (\mathbf{X}'_0 - \mathbf{X}''_0) - \mathbf{C}''(\mathbf{B}.\mathbf{A}.\mathbf{u}'' + \Delta\overline{\mathbf{X}}) = 0.$$

This is a set of three equations in two unknowns λ', λ'' or $\overline{\Omega}'$, $\overline{\Omega}''$, respectively. To obtain the model coordinates, it would be required to first compute corrections to the entities considered as observations and subsequently determine the unknown.

Eliminating from the original 6 equations with 5 unknowns the λ', λ'' or $\overline{\Omega}'$, Ω'', respectively a more effective procedure would result, since the solution of the remaining system of 4 equations in three unknowns gives directly the three model coordinates. For angle measuring sensors, this procedure would be analogous to the photogrammetric formulation by means of the collinearity conditions. For echotime measuring sensors, however, the reduced equations are the non-linear ones given as formula (2).

Another way of computing model coordinates is to choose three out of the four equations in the three unknown model coordinates and to solve the three equations without overdetermination. The selection of the three equations must be such that the determinant of the coefficient matrix is possibly large. For the case of echotime measurement, the equations are non-linear, so that more than one solution will result. Replacing one of the three selected equations by the remaining fourth (again such that the coefficient matrix does not approach singularity), another (group of) solution(s) will be provided. For the example of echotime measurements, this can be geometrically interpreted in the following way (see also Konecny [5]): Two spheres (formula (2a)) are intersected, producing a circle. This circle is intersected

first with one cone (formula (2b)) having its vertex at one sensor position and producing (in the general case) four points of intersection. Intersecting it then with the other cone (vertex at other sensor position), again four points will be defined. Only one point will coincide in both solutions, being the proper one. Taking the arithmetic mean of both will improve the final accuracy.

4. *Cofactors of model coordinates*

The quality of model coordinates as derived from remote sensing imagery, can be judged by means of the matrix of cofactors, $\mathbf{Q}_x$. For this purpose a limited numerical investigation has been performed, in which $\mathbf{Q}_x$ was determined with the law of error propagation. As input was given the matrix of weight coefficients of the measured entities, $\mathbf{Q}_e$. The investigation was limited to the 4 schematical flight configurations of figure 2 and continuous imagery of the direction and echotime-measuring type.

4.1 *The computation method*

A large number of possibilities is available to compute the vector $\mathbf{X}$ from a pair of groups of equations of type (1).

For the present numerical investigation, the original two groups of equations (1) were reduced to only 4 equations in the three unknown model-coordinates. This was interpreted then as an adjustment problem according to Standard Problem IV:

$$ {}_4\mathbf{A}_{14} \cdot {}_1\mathbf{v}_{14} + {}_4\mathbf{B}_3 \cdot {}_1\mathbf{X}_3 + {}_1\mathbf{w}_4 = 0 $$

with $\mathbf{v}$ being the corrections to the observed quantities, $\mathbf{X}$ the unknowns, $\mathbf{w}$ the contradictions and $\mathbf{A}$ and $\mathbf{B}$ as coefficient matrices.

Thus the matrix of cofactors of $\mathbf{X}$, $\mathbf{Q}_x$, results as:

$$ \mathbf{Q}_x = (\mathbf{B}^T (\mathbf{A}\, \mathbf{Q}_e\, \mathbf{A}^T)^{-1}\, \mathbf{B})^{-1} $$

This rigourous method can be compared with the simplifying procedure as described in section 3.3, which gives the unknown model coordinates as the arithmetic mean of the two determined solutions:

$$ (\mathbf{X}) = {}^1/_2\, (\mathbf{X}_1' + \mathbf{X}_2') $$

$\mathbf{X}_1'$, $\mathbf{X}_2'$ result each from solving only three out of the four equations, in the way as mentioned in section 3.3. The cofactors of $(\mathbf{X})$ then are

$$ (\mathbf{Q}_x) = {}^1/_4\, (\mathbf{Q}_{x1} + \mathbf{Q}_{x2} + \mathbf{Q}_{x1x2} + \mathbf{Q}_{x2x1}) $$

It can be shown that $\mathbf{Q}_x$ and $(\mathbf{Q}_x)$ are identical for certain flight configurations. This is explained for the example of SLAR, scheme (b): The left strip of imagery defines, as the locus of each imaged point, the intersection of a sphere (see equation (2a)) with a cone (2b).

Assuming the vertex angle of the cone to be 180^0, this degenerates to a plane. The right strip of imagery is defining another sphere and plane. For the scheme (b) now, the two planes coincide, so that two of the 4 equations in the unknowns X, Y and Z are identical. Obviously then $\mathbf{Q}_x$ and $(\mathbf{Q}_x)$ are identical too.

φ^o_o		Y=0	Y=.75	Y=1.5
2.5	Qx	0.6	0.6	0.8
	Qy	0.7	185	899
	Qz	304	328	399
10	Qx	0.6	0.6	0.8
	Qy	0.7	12.2	568
	Qz	19.0	20.5	25.0
30	Qx	0.7	0.7	0.9
	Qy	0.7	2.0	6.9
	Qz	2.1	2.3	2.8

Scheme (a)
plane scan

ϕ^o_o		Y=0	Y=.75	Y=1.5
2.5	Qx	0.6	0.6	0.8
	Qy	0.7	119	277
	Qz	304	210	123
10	Qx	0.6	0.6	0.8
	Qy	0.7	8.0	18.0
	Qz	19.0	13.3	8.2
30	Qx	0.7	0.8	1.1
	Qy	0.7	1.5	2.7
	Qz	2.1	1.7	1.5

Scheme (a)
conical scan

by		Y=0	Y=.75	Y=1.5
0.5	Qx	o.6	o.6	o.7
	Qy	1.3	3.6	45.2
	Qz	11.7	13.6	31.8
1	Qx	0.6	0.6	0.7
	Qy	1.3	0.9	4.9
	Qz	4.0	3.4	6.9
1.5	Qx	0.7	0.6	0.7
	Qy	1.3	1.0	1.3
	Qz	2.9	1.8	2.9

Scheme (b)

bz		Y=0	Y=.75	Y=1.5
1	Qx		0.7	0.9
	Qy		12.9	22.7
	Qz		33.6	17.1
2	Qx		0.8	1.0
	Qy		10.1	13.9
	Qz		25.1	10.9
3	Qx		0.9	1.1
	Qy		11.8	14.3
	Qz		26.9	10.3

Scheme (c)

Table 3/1: Cofactors of modelcoordinates, derived from overlapping imagery produced by optical mechanical scanning. *Y, bx, by* and *bz* are given as multiples of the flying height

4.2 *Results*

$\mathbf{Q}_x$ has been computed under various assumptions for the base $\mathbf{b} = (\mathbf{X}_0'' - \mathbf{X}_0')$, the angle $2\varphi_0$ for convergence, the squint Φ_0, the angle α between two corresponding flight lines and the position of point P. The unit of measurement was the flying height $(Z_0' - Z_P)$. The ratio among cofactors of the observed entities $(\mathbf{X}_0, \varphi, \omega, \varkappa)$ as well as s for SLAR has been assumed as:

$$Q_{x0}:Q_{y0}:Q_{z0}:Q_\varphi:Q_\omega:Q_\varkappa:Q_s = 1:1:0.2:0.04:0.04:0.04:0.5.$$

For the optical mechanical scanning it was assumed that the base is defined more accurately due to the better geometric resolution and the larger scale. Furthermore, the orientation of the sensor is supposed to be known to a lesser degree of precision due to the fact that it is a comparatively less expensive sensor, so that

$$Q_{x0}:Q_{y0}:Q_{z0}:Q_\varphi:Q_\omega:Q_\varkappa:Q_\Omega = 1:1:0.4:0.16:0.16:0.16:0.16.$$

4.2.1 *Optical-mechanical scanner*

After computation of the spatial coordinates, one obtains their weight coefficients as given in tables 3. It turns out, that the X-model coordinates can be well determined by imagery from all schemes with parallel flight lines (schemes (a) — (c)), whereas the cofactors of the Y- and Z-coordinates become the smallest with the "opposite-side" stereo arrangement of scheme (b). For the heights therefore, the scheme (b) is considered to be optimum as far as error propagation is concerned, and gives the best values for Z in the middle of the overlapping area ($Q_z \approx 1.8$ for by $= 1.5\ H$, from scheme (c)).

bx		Y=0	Y=.75	Y=1.5
0	Qx		0.6	0.7
	Qy		1.2	1.2
	Qz		5.6	2.9
0.75	Qx	1.2	1.0	1.1
	Qy	0.6	1.0	1.2
	Qz	5.6	2.9	2.0
1.5	Qx	1.2	1.2	1.3
	Qy	0.7	1.1	1.3
	Qz	2.9	2.0	1.5

Scheme (d)

Table 3/2: Cofactors of modelcoordinates, derived from overlapping imagery produced by optical mechanical scanning. Y, bx, by and bz are given as multiples of the flying height (cont'd)

The idea of convergent "stereosystems", considered as a promising concept to overcome the mapping difficulties with remote sensing systems, and including the alternative of rectilinear or hyperbolic scanning is disappointing (tables (a), (b)). In comparison to other imaging arrangements, the error propagation into Y- and Z-coordinates is very unfavourable. A small angle of convergence ($2\varphi_0 = 5^0$) with rectilinear scan does produce along the edge of the imaged area cofactors of extreme size. For $2\varphi_0 = 20^0$, these reduce to $Q_y = 57$, $Q_z = 25$, but only for $2\varphi_0 = 60^0$, the cofactors take on acceptable values of $Q_y = 7$, $Q_z = 3$.

The hyperbolic scan is clearly producing more accurate results, but can not, with the small convergence angles, reach the ones obtainable by scheme (b). Y is by far less precisely defined than Z. What is then the use of this concept? It is the possibility of carrying out a strip triangulation, which should allow for a better determination of the data of exterior orientation than the direct measurement. But from Derenyi's investigation [2] the conclusion can be drawn that relative orientation is not promising (see section 3.1). And even under the hypothetical assumption that the relative orientation could provide more accurate data for exterior orientation than direct measurement as assumed above, then still the resulting cofactors are very large, even for the example of the more accurate hyperbolic scan.

Table 3(b) demonstrates in addition, that Q_z decreases with increasing distance between P and the flight line — which is the opposite of the case of Q_y. This is caused by the increase of the base-height-ratio, which overcompensates the deteriorating effect of the reduced image scale (or resolution) with increasing Y.

"Same side stereo" as realized in scheme (c) with parallel flight lines above each other (table 3(c)) does not allow the computation of heights along the flight track to be carried out: Z is not defined. The inaccuracy of Y-coordinates increases with the distance from the flight track. From table 3(d) it can be concluded that, for a given set of cofactors for the observed quantities, there is an optimum bz: $1 < bz < 3$. An interesting configuration is scheme (d), which defines X and Y with cofactors smaller than, or equal to 1.

The accuracy of Z increases with increasing Y, but is similar to that from scheme (b).

There is no correlation between the model coordinate X and (Y, Z), except for scheme (d), while Y and Z are strongly correlated. There is no loss of accuracy when applying the simple arithmetic mean from the two determined solutions, except for scheme (d).

We may then conclude that:

The superior flight configuration is the "opposite side"-case, indicated as scheme (b). Comparable accuracy can only be expected from scheme (d). The application of convergent systems does not lead to improvements in metric accuracy, especially with small convergence angles ($2\varphi_0 \leqslant 20^0$).

4.2.2 *Side-Looking-Radar*

The cofactors of SLAR-model coordinates are generally larger than the ones for the optical-mechanical scanner.

As is obvious from table 4, the X coordinate is well defined in all flight configurations, whereas the heights cannot be satisfactorily determined, except for one case. Considering Q_z in scheme (b), it turns out that it becomes rather large in the centre of the model area. Under the abovementioned assumptions, Q_z reaches a values of 34. Along the edge of the model area only can a Q_z be expected of a size near the error of unit weight. But it is exactly there where the qualitative usefulness

φ^o_o		Y=1	Y=2.5	Y=5
2.5	Qx	0.5	0.6	1.0
	Qy	283	54.8	22.1
	Qz	283	338	536
10	Qx	0.5	0.6	1.0
	Qy	17.7	4.0	2.1
	Qz	17.4	20.9	33.4
30	Qx	0.6	0.7	1.2
	Qy	2.1	1.0	0.9
	Qz	1.7	2.1	3.6

Scheme (a)

by		Y=1	Y=2.5	Y=5
5	Qx	0.7	0.6	0.7
	Qy	1.1	0.8	1.6
	Qz	2.4	5.0	0.7
10	Qx	0.9	0.9	1.0
	Qy	1.2	1.0	0.8
	Qz	3.2	11.1	19.2
15	Qx	1.0	1.1	1.5
	Qy	1.3	1.1	0.8
	Qz	3.2	13.5	33.7

Scheme (b)

bz		Y=1	Y=2.5	Y=5
1	Qx	0.6	0.7	1.0
	Qy	13.1	8.4	7.7
	Qz	6.5	22.2	78.5
5	Qx	0.7	0.9	1.3
	Qy	4.2	2.5	2.3
	Qz	1.2	1.8	4.0
10	Qx	0.9	1.1	1.6
	Qy	3.5	2.1	1.9
	Qz	0.9	1.0	1.6

Scheme (c)

bx		Y=1	Y=2.5	Y=5
1	Qx	0.9	1.2	2.0
	Qy	0.9	0.7	0.7
	Qz	1.6	2.9	4.0
5	Qx	0.7	0.8	1.5
	Qy	2.0	1.8	1.5
	Qz	4.0	17.2	44.6
10	Qx	0.6	0.8	1.2
	Qy	4.9	4.5	3.8
	Qz	7.0	36.2	112

Scheme (d)

Table 4: Cofactors of modelcoordinates, derived from overlapping side-looking radar imagery. Y, bx, by and bz are given as multiples of the flying height

of SLAR-imagery is limited (see: $by = 5$, $Y = 5$, table 4b). Scheme (c) can produce more accurate Y-coordinates with increasing distance from the flight track. Q_z obviously deteriorates in this direction. A larger bz reduces the size of Q_y and Q_z, whereas Q_x increases slightly.

With cross-strips (scheme (c)) there is a good definition of the model point in the vicinity of the flight lines only. With increasing bx and the object point in the distant corner of the model area, the Q_z deteriorates rapidly (e. g. $Q_z > 100$ for $bx = 10.H$, $Y_p = 5.H$).

Also for the SLAR-principle there exists the possibility to arrange a convergent system such as to obtain overlapping imagery. In section 3.2 it was mentionned, that the conical convergence, as applicable in the optical-mechanical scanner, does not define a model point. Only by forward and backward directed oblique plane impulses, so that $\varphi_0 \neq 0$, a model can be formed with a convergent SLAR-system. An angle of convergence of 20^0 still gives disappointing results (table 4a). For $2.\varphi_0 = 60^0$, however, the cofactors improve to satisfactory values. Q_z even becomes in this case superior to the corresponding values obtainable by all other configurations. The question remains, how a convergence of 60^0 affects the interpretability of the imagery.

With reference to the correlation among the model coordinates the following results may be drawn: X is not correlated with Y and Z, exept for scheme (d). Y and Z are strongly correlated. Neglecting this correlation and computing Y and Z as simple arithmetic mean of the two solutions Y_1, Y_2, Z_1, Z_2, should, for configuration (d), be avoided.

So the conclusion is:

Planimetric plotting can best be done with schemes (b) or (a), the latter with large angle of convergence ($\sim 60^0$). Plotting of heights with the highest accuracy is possible with the last configuration.

4.2.3 *Combination of Continuous Echotime and Direction Measuring Sensors*

When considering the model formation from overlapping imagery of differing characteristics, then one should not forget, that such a combination is doubtful for the following reason: the measurement of direction is most accurate right below the sensor, at a depression angle of 90^0, whereas the measurement of echotime satisfactorily resolves terrain details only at depression angles other than 90^0, thus up to 75^0. The resolution properties are very different, so as the size and location of the imaged area with respect to the flight line are not similar in both systems.

For their combination, therefore, none of the proposed flight configurations could be considered an operational arrangement to produce overlapping imagery.

However, for the purpose of computing model coordinates, there exists the realistic possibility to supplement a SLAR-strip with depression angles from a simultaneous radar interferometer. This differs from the other configurations menti-

oned in sections 4.2.1 and 4.2.2, since there is no overdetermination through superfluous projection equations.

y	1	1.5	2.5	5
Q_x	1.3	1.5	2.2	5.2
Q_y	1.6	1.7	1.7	1.8
Q_z	1.0	1.3	2.5	8.4

Table 5: Cofactors of model coordinates derived from a system measuring simultaneously echo time and depression angle (Read Y instead of y)

Table 5 shows the results for such an arrangement for the following weight assumptions:

$$Q_{x0}:Q_{y0}:Q_{z0}:Q_\varphi:Q_\omega:Q_\varkappa:Q_s:Q_\Omega = 1:1:0.4:0.16:0.16:0.16:0.5:0.16$$

where Y is determined rather well. In judging the numerical values, one has to bear in mind, that, besides the lack of overdetermination, the weight coefficients for the observations differ from those assumed for tables 3 and 4.

5. *Conclusions, Recomendations*

In the investigation of the model formation with remote sensing imagery the present study starts from a general projection equation, which can be specialised for the various imaging systems. The model coordinates in these equations are expressed as functions of quantities, which are assumed to be measured. The effect of various flight configurations to obtain overlapping imagery for given accuracies of measurable quantities is studied. By means of the law of error propagation, the cofactors of the model coordinates are computed for the optical mechanical scanning, the side looking radar and a combination of these two principles.

The main conclusions can be drawn from the self explanatory tables. However, one may summarize these on the basis of error propagation

(i) for optical mechanical scanning:
- — scheme (b) allows for the best model formation;
- — X-coordinates are well determined in all configurations;
- — the convergent systems are disappointing; the errors propagate unfavourably into model coordinates;
- — hyperbolic scanning is superior to rectilinear scanning for convergent systems;

— there is no correlation of X with Y- and Z-coordinates, except for scheme (d); Y and Z are strongly correlated;

(ii) for the echotime measurement:
- scheme (b) allows for the best model formation; heights are only inaccurately defined in the middle of the model area;
- X-coordinates are generally well defined;
- cross strips (scheme (d)) do not improve the model coordinates with respect to error propagation;
- convergent SLAR-systems are disappointing; they only could be successful if large convergence angles are applied, e. g. 60^0;
- with regard to correlation among the model coordinates the same holds as for optical mechanical scanning;

(iii) for a combination of both principles:
- the physical difference of the sensors hampers the realisation of the geometrical concept;
- the measurement of the depression angle with a radar interferometer would give model coordinates of relatively high and homogenous accuracy.

With regard to further investigations it is advisable, on the basis of the obtained results, to stress concepts (a) and (b) of figure 2. It would be desirable to perform a practical test using real imagery. This, however, is only possible for scheme (b), since appropriate convergent systems with large convergence angles are not available at the present time.

The numerical values in the tables 3—5 should, as far as their absolute size is concerned, be interpreted with care since they are based on rather arbitrary assumptions for the weight coefficients of the observed quantities. Some photogrammetrists may certainly consider the resulting values for the cofactors of the model points rather large. However, the values as given in the tables concern absolute accuracy, and the coordinate errors of neighbouring points are correlated, so that control points may improve the absolute accuracy.

Further study should therefore be devoted to the implementation of stochastic filtering and interpolation of the errors of model coordinates.

Acknowledgement

I am very grateful to Prof. Dr. E. M. Mikhail for critically reading the manuscript and valuable suggestions regarding sections 3.3 and 4.1 on the method of computing model coordinates.

Appendix: height accuracy obtained from optical-mechanical scanning

Convergent plane scan

The height h of a point B with reference to a datum through point A is defined in figure 3 and can be computed by means of

$h = \Delta P/(2.\tan \varphi_0)$ ΔP ... Parallax difference

where

$$\Delta P = P_A - P_B = p_A.\lambda_A - p_B.\lambda_B \qquad P \ldots \text{Parallax}$$

The scale of the imagery, λ, is variable in y-direction:

$$\lambda = \frac{H}{c} \cdot \left(\frac{1}{\cos^2 \varphi_0} + \tan^2 \Omega \right)^{1/2}$$

The measurement of the parallax difference consists of the observation of the x-coordinates of A', A'', B', B''. Assuming a mean observational error σ_0 in the photograph, this will lead to

$$m^2 (P_A) = 2\sigma^2{}_0 . H^2 / (c^2 . \cos^2 \varphi_0)$$

$$m^2 (P_B) = 2\sigma^2{}_0 . \frac{H^2}{c^2} \cdot \left(\frac{1}{\cos^2 \varphi_0} + \tan^2 \Omega_B \right)$$

Thus

$$m^2 (\Delta P) = \sigma^2{}_0 . \frac{H^2}{c^2} . 2 . \left(\frac{2}{\cos^2 \varphi_0} + \tan^2 \Omega_B \right)$$

Taking the square root gives

$$m(h) = \frac{\sigma_0 . H . (\cos^2 \varphi_0 . \tan^2 \Omega_B / 2 + 1)^{1/2}}{c . \sin \varphi_0}$$

Convergent conical scan

Here, h results from

$$h = \Delta P . \cos \Omega_B / (2 . \tan \Phi_0) - H . \cos \Omega_B \left(1 - \frac{1}{\cos \Omega_B} \right)$$

The same consideration as above then obviously leads to

$$m(h) = \frac{\sigma_0 . H . (\cos^2 \Omega_B + 1)^{1/2}}{\sqrt{2} . \sin \Phi_0 . c}$$

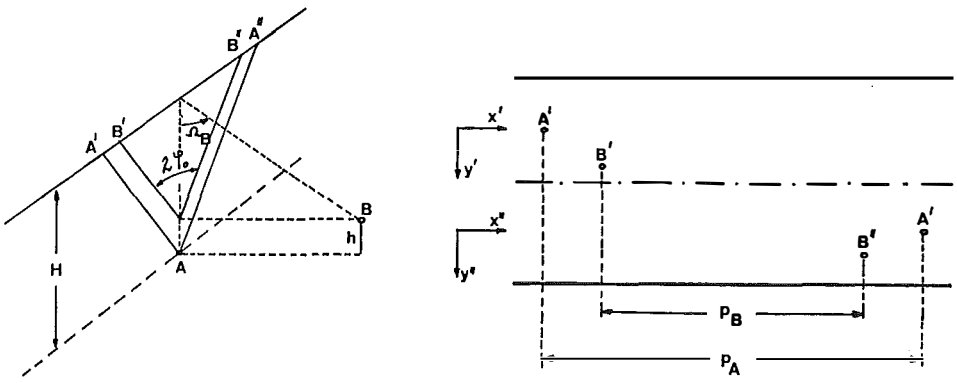

Figure 3: Definitions for derivation of height accuracy from convergent optical mechanical scanner

Literature

[1] *Case, J. B.:* "The Analytical Reduction of Panoramic and Strip Photography", Photogrammetria, Vol. 22, pp. 127, 1967.

[2] *Derenyi, E. E.:* "Relative Orientation of Continuous Strip Photography", Univ. of New Brunswick, Canada, 1970.

[3] *Elms, D. G.:* "Mapping with a Strip Camera", Photogrammetric Engineering, Vol. XXVIII, 1962.

[4] *Hockeborn, H. A.:* "Extraction of Positional Information from Side-Looking Radar", ISP-Symposion, Comm. II, Munich, 1970.

[5] *Konecny, G.:* "Metric Problems in Remote Sensing", ISP-Symposion, Comm. IV, Delft, 1970, in: ITC-publ. series A nr. 50.

[6] *LaPrade, G. L.:* "An Analytical and Empirical Study of Stereo for Radar", Photogrammetric Engineering, Vol. XXIX, 1963.

[7] *LaPrade, G. L.:* "Subjective Considerations for Stereo Radar", Goodyear Aerospace Corp., Gib-9169, 1970.

[8] *Levine, D.:* "Radargrammetry", McGraw Hill, 1960.

[9] *Masry, S. E:* "Analytical Treatment of Stereo Strip Photos", Photogrammetric Engineering, Vol. XXXV, 1969.

[10] *Moore, R. K.:* "Heights from Simultaneous Radar and Infrared", Photogrammetric Engineering, Vol. XXXV, 1969.

[11] *Moura, J. M. de:* "Project RADAM of the Ministry of Mines and Energy", PR-Conselho Nacional de Pesquisas, Inst. de Pesquisas Espacias, INPE, Sao José dos Campos-SP-Brasil, 1971.

[12] *Miranda, A.:* "Radar Stereo Equipment", Goodyear Aerospace Corp., Gib-9198, 1970.

[13] *Norvelle, F. Raye:* "AS-11-A Radar Program", Photogrammetric Engineering, Vol. XXXVIII, 1972.

[14] *Rosenfield, G. H.:* "Stereo Radar Techniques", Photogrammetric Engineering, Vol. XXXIV, 1968.

[15] *DiCarlo, C., DeMeter, E.:* "DoD Data Processing Equipment for Radar Imagery", United States Department of Defense, Paper presented to FIG Congress, Wiesbaden, W.-Germany, 1971.

A Theoretical Random-Error Propagation Law for Anblock-Networks With Constrained Boundary

By *P. Meissl*, Vienna

Zusammenfassung

Anblocknetze setzen sich aus einer großen Anzahl aneinanderliegender elementarer Figuren zusammen. Für jede Figur liegen separate photogrammetrische Messungen vor, die es gestatten, die Gestalt der Figur in einem unbekannten Maßstab zu rekonstruieren. Ebner hat für große idealisierte Anblocknetze mit festgehaltenen Randpunkten mittels Computer numerische Fehlerstudien durchgeführt. An Hand seiner Resultate vermutete er, daß der durchschnittliche Koordinatenfehler nach strengem Ausgleich einem ähnlichen logarithmischen Gesetz folgend mit der Anzahl der Netzpunkte anwächst, wie dies vom Autor im Falle großer Nivellementnetze nachgewiesen wurde. Ebners Vermutung wird hier auf analytischem Wege bewiesen. Die genaue Form des asymptotischen Fehlergesetzes wird gefunden.

Summary

Anblock-networks are composed of a large number of adjacent elementary figures. For each figure separate photogrammetric measurements are taken, allowing to reconstruct the shape of the figure in an unknown scale. Ebner has performed computer simulation studies for large idealized